Frequency-resolved optical gating for time-resolving knockout in double ionization with attosecond pulses

H. Price,[1] A. Staudte,[2] P. B. Corkum,[2] and A. Emmanouilidou[1,3]

[1]*Department of Physics and Astronomy, University College London, Gower Street, London WC1E 6BT, United Kingdom*

[2]*Joint Laboratory for Attosecond Science, University of Ottawa and National Research Council, 100 Sussex Drive, Ottawa, Ontario K1A 0R6, Canada*

[3]*Chemistry Department, University of Massachusetts at Amherst, Amherst, Massachusetts 01003, USA*

(Received 26 July 2012; published 16 November 2012)

We develop the two-electron attosecond streak camera under realistic conditions using a quasiclassical model. We assume extreme ultraviolet (XUV) attosecond pulses with a full width at half maximum (FWHM) of 24 attoseconds, centered at 120 eV and a streaking infrared laser field of 1600 nm, and intensity of 1.8×10^{12} W/cm^2. The proposed method is shown to be capable of time resolving two-electron collisions in double ionization.

DOI: 10.1103/PhysRevA.86.053411 PACS number(s): 32.80.Fb

I. INTRODUCTION

Time-resolving correlated electron processes is one of the driving forces behind the large-scale effort to push the frontiers of attosecond science. Attosecond science offers time resolution through extreme ultraviolet (XUV) pulses. However, pump-probe experiments using attosecond pulses are technically very challenging. Hence, the streaking of photo-electrons with an infrared (IR) laser field has become a successful technique for bringing time resolution to photoionization. The paradigmatic attosecond streak camera [1,2], and its development into FROG CRAB (frequency resolved optical gating for complete reconstruction of attosecond bursts) [3], which originally aimed to characterize attosecond XUV pulses, have been the underlying concepts for studies resolving delayed time emission from atoms [4–8] and solids [9].

To study the electron correlation in single-photon double ionization we recently formulated the two-electron streak camera [10]. Specifically, it was shown that the intra-atomic knock-out process [11] can be associated with a delay, that is, a time between photoabsorption and ejection of two electrons in the continuum. The delay is encoded in the interelectronic angle of escape as a function of the phase of the IR laser field. In addition, the two-electron streak camera can time resolve delays corresponding to different energy sharings, between the two electrons, and to different ionization mechanisms [12]. However, previous work considered only discrete photon energies and instantaneous photoabsorption [10,12].

Here, we remove this severe limitation and extend the two-electron streak camera to realistic attosecond pulses. By resolving the bandwidth of an XUV pulse in the sum energy of two emitted electrons, we construct the two-electron equivalent of FROG to obtain a complete picture of the single-photon double-ionization process. Specifically, in FROG [13] one extracts from a two-dimensional data set (FROG trace) the complete characteristics of an optical pulse. In a similar manner in FROG CRAB [3] one retrieves the spectral phases and amplitudes of an attosecond pulse. Here, we assume a transform-limited XUV attosecond pulse to obtain information about the delay of two-electron emission after absorption of a photon from the attosecond pulse. We use the interelectronic angle of escape as a function of the phase of the IR laser field as FROG-like trace for double ionization. We devise a simple algorithm for extracting the two-electron delays for different excess energies.

II. METHOD

We build on our classical trajectory Monte Carlo [14] simulation of the classical He*$(1s2s)$ model system, described in detail in Refs. [10,12,15–17]. Briefly, we classically propagate the Coulomb three-body problem using the classical trajectory Monte Carlo (CTMC) phase space method. CTMC has often been used to describe breakup processes induced by particle impact [18] with implementations differing usually in the way the phase space distribution of the initial state is constructed. We use a Wigner transform of the initial quantum wave function for the initial state, and this is why we call our approach "quasi"-classical. Naturally, the electron-electron interaction is treated to all orders in the propagation, and any difficulties with electron correlation in the final state are absent, since the method is explicitly time dependent.

We choose He*$(1s2s)$ as a prototype system to clearly formulate the concept of streaking two-electron dynamics while avoiding the unnecessary complexity of many-electron and multicenter systems. However, the scheme is not system specific and can time resolve two-electron collisions mediated by the knock-out mechanism. For atoms, knock out and shake off are the two well-established mechanisms underlying two-electron escape after a single photon is absorbed; the former mechanism dominates for small excess energies and the latter mechanism for large ones [11]. For instance, our scheme can be used to time resolve the collision between $1s$ and $2s$ electrons in the ground state of Li [15–17]. In addition, it can be used to time resolve two-electron collisions taking place in molecular systems such as the He dimer where single-photon double ionization was shown to be mediated by a knock-out process [19]. Atomic units (a.u.) are used throughout this work except where otherwise indicated.

Figure 1(a) illustrates the concept of the two-electron streak camera. First, the $1s$ electron (photoelectron) absorbs the XUV attosecond pulse with energies above the double-ionization threshold. Then, as the electron leaves the atom it can collide

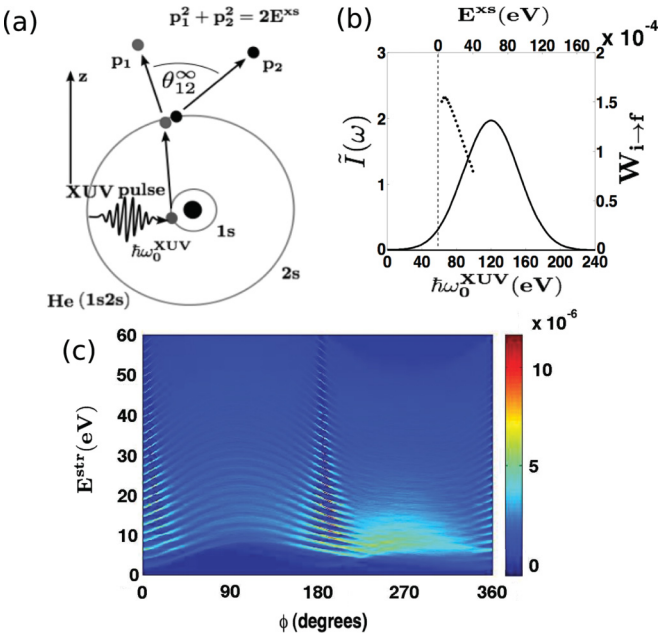

FIG. 1. (Color online) (a) Sketch of the intra-atomic knock-out mechanism to be studied with the two-electron streak camera. The streaking field causes a decrease in θ_{12}^{∞} when the photoelectron is launched along the $+\hat{z}$ direction, since adding $\Delta p_{\rm IR}$ to each of the electron momenta results in $\theta_{12} < \theta_{12}^{\infty}$. (b) Spectral intensity of the XUV pulse scaled by $(F_0^{\rm XUV})^2$. Dotted curve: $W_{i\to f}$ in the presence of the XUV and IR field averaged over all $\phi's$. (c) Observable $E^{\rm str}$ total electron energy as a function of ϕ considering excess energies from 4 to 60 eV in steps of 2 eV and double-ionization events corresponding to launching of the photoelectron ($1s$) in the $\pm\hat{z}$ direction for ϕ ranging from 0° to 180°. To illustrate the difference between launching of the photoelectron in the $+\hat{z}$ versus the $-\hat{z}$ direction we plot the $E^{\rm str}$ corresponding to $+\hat{z}$ for ϕ ranging from 0° to 180° and the $E^{\rm str}$ corresponding to $-\hat{z}$ for ϕ ranging from 180° to 360°.

with the $2s$ electron and transfer some of its energy, resulting in the simultaneous ejection of both electrons. The intra-atomic collision is typically characterized by the asymptotic inter-electronic angle of escape, θ_{12}^{∞}, that can be observed by experiment [11]. To time resolve the two-electron collision dynamics we streak θ_{12}^{∞} by adding a weak IR laser field polarized along the z axis, $\vec{F}^{\rm IR}(t) = F_0^{\rm IR} f(t)\cos(\omega_{\rm IR}t + \phi)\hat{z}$, where ϕ is the phase between the IR field and the XUV pulse and $f(t)$ is the pulse envelope [10]. We choose $\omega_{\rm IR} = 0.0285$ au (1600 nm) and $F_0^{\rm IR} = 0.007$ a.u. ($<1.8 \times 10^{12}$ W/cm^2) so that the streaking field does not alter the attosecond collision significantly but still has an observable effect on θ_{12}. Here, $F_0^{\rm IR} = 0.007$ a.u. is chosen to efficiently streak excess energies from 10 to 60 eV. The IR laser field splits $\theta_{12}(\phi)$ in two branches with the lower (upper) branch corresponding to launching of the photoelectron along the $+z$ ($-z$) direction; see Fig. 1(a).

Next, we describe how we model the XUV attosecond pulse and how its spectral intensity needs to be reflected in the weight of trajectories corresponding to different excess energies. The electric field of the XUV pulse is of the form

$$\vec{F}^{\rm XUV}(t) = F_0^{\rm XUV} e^{-t^2/4\sigma^2}\cos\left(\omega_0^{\rm XUV} t\right)\hat{z} \qquad (1)$$

with σ the standard deviation of the temporal intensity envelope $I(t)$. For the current calculations, the spectral intensity $\tilde{I}(\omega)$ of the XUV pulse has a FWHM of 75 eV, centered at $\omega_0^{\rm XUV} = 120$ eV; see Fig. 1(b). The temporal intensity envelope $I(t)$ of the transform limited pulse has a FWHM of 1 a.u.. In what follows we focus on the effect the large-energy bandwidth of the XUV pulse has on the streaking process and we neglect the effect of the finite FWHM of $I(t)$. The uncertainty of the time of photoabsorption will be taken into account after the application of the streak camera algorithm as an uncertainty in the retrieved delay times.

Using first-order perturbation theory we compute the photoabsorption probability to transition from the initial ground state of He*($1s2s$) to the final state of double-electron escape [20]:

$$W_{i\to f} \propto \frac{1}{\omega}\sigma^{2+}(\omega)\tilde{I}(\omega) \qquad (2)$$

with the cross section for double ionization $\sigma^{2+}(\omega)$ given by $\sigma_{\rm abs}(\omega)P^{2+}(\omega)$. $\sigma_{\rm abs}$ is the cross section for photoabsorption which we calculate in the single-electron approximation, assuming that the $1s$ electron absorbs the photon [21]. $P^{2+}(\omega)$ is the probability for double ionization obtained through our classical simulation [10,15,16]. Finally, we weight each classical trajectory for a given photon energy ω by the factor $\sigma_{\rm abs}(\omega)\tilde{I}(\omega)/\omega$.

III. RESULTS

Our goal is to retrieve the delay between photoabsorption and ionization of both electrons. Since the delay depends on the sharing of the final energy among the two electrons [10], we consider in the following only symmetric energy sharing of $\epsilon < 0.14$. The delay times for the most symmetric energy sharing correspond roughly to the time of minimum approach of the two electrons, that is, to the collision time. Here, we have defined the energy sharing, $\epsilon = (\epsilon_1 - \epsilon_2)/(\epsilon_1 + \epsilon_2)$, as the dimensionless asymmetry parameter between the (final) kinetic energies ϵ_1 and ϵ_2 of the two electrons. In what follows, we consider the symmetric sharing with respect to the streaked or the "modified" electron energy—both energies are defined in what follows. The analysis of different energy sharings as described in Ref. [12] can be applied to the following analysis without any restrictions. In Fig. 1(c) we plot a FROG-like trace for two-electron ejection, the observable total electron energy in the presence of the XUV plus IR laser field, $E^{\rm str}$ (streaked energy), as a function of ϕ for excess energies ranging from 4 to 60 eV in steps of 2 eV. Figure 1(c) is plotted for symmetric $E^{\rm str}$ energy sharing. In what follows, we describe how we extract from Fig. 1(c) the delay times of the intra-atomic two-electron collisions for different triggering excess energies. The excess energy is given by $E^{\rm xs} = \omega - I_p$, where I_p is the ionization potential of the model He*($1s2s$) system.

We first study the effect of the large energy bandwidth of the XUV pulse on streaking the two-electron collision dynamics. In Fig. 2(a) we plot the correlation map of the excess energy of the XUV photon and the observable sum energy $E^{\rm str}$ of both electrons. We see that a large range of excess energies maps to the same streaked total electron energy. Hence, the final electronic state does not correspond unambiguously

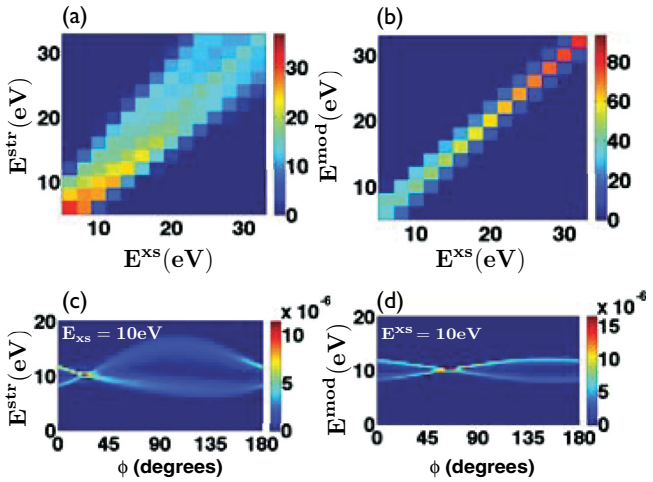

FIG. 2. (Color online) Correlation map of the excess energy E^{xs} (a) with the observable electron energy E^{str} and (b) with the "modified" electron energy E^{mod}. The color scale in panels (a) and (b) is such that the sum of E^{xs} contributing to a certain E^{str} is normalized to 100. (c) Streaked electron energy and (d) "modified" electron energy as a function of ϕ for $E^{xs} = 10$ eV excess energy. Panels (a) and (c) are plotted for symmetric E^{str} energy sharing while panels (b) and (d) are plottedfor symmetric E^{mod} energy sharing.

to the triggering excess energy. For instance, the 20 eV streaked energy maps to excess energies ranging from 12 to 26 eV. The reason for the weak correlation between the streaked and the excess energy becomes clear in Fig. 2(c) for 10 eV excess energy: the streaked energy changes significantly with ϕ.

To retrieve the excess energy from the final electronic state with improved accuracy, we introduce a "modified" total electron energy, where the effect of the streaking IR field is reduced. Therefore, we define a "modified" electron momentum p_i^{mod} by subtracting the momentum change Δp_{IR} due to the streaking IR field, that is,

$$\mathbf{p}_i^{mod} = \mathbf{p}_i^{str} - \Delta p_{IR}\hat{z}, \tag{3}$$

where the index $i = 1,2$ labels the two electrons. The change in momentum due to the streaking field (neglecting the Coulomb potential) is given by

$$\Delta p_{IR} \approx \frac{F_0^{IR}}{\omega_{IR}} \sin(\Delta\phi + \phi). \tag{4}$$

Here, the shift $\Delta\phi = \omega_{IR} t_{delay}$ with respect to the maximum of the vector potential of the IR field, $A_{IR}(\phi)$, is due to the delayed electron emission; see Ref. [10] for more details. Since we want to retrieve t_{delay} we set $\Delta\phi = 0$ when computing the "modified" electron momentum p_i^{mod}. Hence, $\Delta p_{IR} \approx \frac{F_0^{IR}}{\omega_{IR}} \sin\phi$. Thus, the "modified" energy E^{mod} corresponding to a certain triggering photon excess energy is given by

$$\sum_{i=1,2} \frac{\left[\left(p_{x,i}^{str}\right)^2 + \left(p_{y,i}^{str}\right)^2\right]}{2} + \sum_{i=1,2} \frac{\left(p_{z,i}^{mod}\right)^2}{2} = E^{mod}. \tag{5}$$

Figure 2(d) shows that the "modified" electron energy varies significantly less with ϕ compared to the unmodified, observable energy E^{str} [Fig. 2(c)]. Consequently, E^{mod} is strongly correlated with the excess energy; see Fig. 2(b). The improved correlation at higher excess energies is likely due to the faster collision; that is, the approximation $\Delta\phi \approx 0$ is better at higher excess energies.

We next explain why at $\phi = 0°(180°)$ the streaked electron energy and as a consequence the "modified" electron energy is smaller (larger) than the corresponding excess energy for photoelectrons ejected in the $+\hat{z}$ direction (it is the other way around for photoelectrons ejected in the $-\hat{z}$ direction). At $\phi = 0°$ each electron experiences a force from the IR field in the direction opposite to the electron's direction of escape. As a result, each electron slows down and escapes with a streaked energy, E^{str}, smaller than the electron's final energy in the absence of the IR field. In contrast, at $\phi = 180°$ each electron experiences a force from the IR field in the same direction as the electron's direction of escape. As a result, each electron escapes with a streaked energy larger than the electron's final energy in the absence of the IR field. To verify that the overall change of the "modified" total electron energy with ϕ is a one-electron effect, we run our simulation in the presence of the XUV plus IR field only for the photoelectron (the 2s electron is absent). Since for the two-electron case we only consider symmetric energy sharing, we compare the two-electron case for a certain excess energy with the one-electron case for half that excess energy. Indeed, multiplying by two the distribution of the one-electron "modified" energy as a function of ϕ for an excess energy of, for example, 5 eV [Fig. 3(a)] and taking the average we find that there is excellent agreement with the two-electron "modified" energy at 10 eV excess energy as a function of ϕ; see Fig. 3(b). Note that in Fig. 3 and in what follows [Figs. 4(b) and 4(d) and Fig. 5] we focus on double ionization events where the photoelectron is ejected in the $+\hat{z}$ direction.

For a certain excess energy, we have shown that the "modified" electron energy increases with ϕ; see Fig. 3(b). This forms the basis for the simple algorithm we develop to determine, for the case when many excess energies are considered (XUV attosecond pulse), the range of "modified" electron energies that pertain to a certain excess energy E^{xs}. Our goal is to select that range of "modified" electron energies that includes all double ionizing events that are triggered by a narrow set of excess energies centered around E^{xs}. The reason is that it is the double-ionization events triggered by a single E^{xs} whose collision time we aim to streak. We label the set of double-ionization events thus selected by $\mathcal{E}^{mod}$.

If our algorithm is dictated mainly by experimentally accessible observables, we compute the collision time corresponding to E^{xs} by selecting the doubly ionizing events whose "modified" electron energy changes from $[E^{xs} - \Delta E/2, E^{xs}]$ eV for $\phi = 0°$ to $[E^{xs} + \Delta E/2, E^{xs}]$ for $\phi = 180°$. We choose ΔE to be roughly 8 eV for all excess energies (method 1). With this selection criterion, the double-ionization events with $\mathcal{E}^{mod} = 10$ eV, enclosed by the white dashed lines in Fig. 3(c), are the events triggered by excess energies ranging from 7 to 13 eV [see Fig. 4 (b)]; these excess energies are indeed roughly centered around $E^{xs} = 10$ eV for all ϕ's. Similarly, the double-ionization events we label by $\mathcal{E}^{mod} = 20$ eV are triggered by excess energies ranging from 17 to 23 eV [see Fig. 4(d)]; these excess energies are roughly centered around $E^{xs} = 20$ eV for all ϕ's.

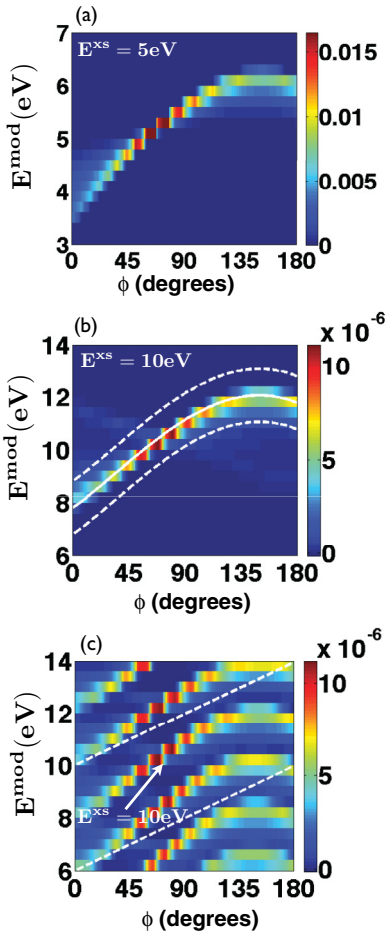

FIG. 3. (Color online) (a) E^{mod} for one-electron as a function of ϕ for 5 eV excess energy. (b) E^{mod} for two electrons as a function of ϕ for 10 eV excess energy; white solid line shows the average of the distribution E^{mod} in (a) times two. (c) E^{mod} for two electrons as a function of ϕ for excess energies between 4 and 14 eV. The white dashed lines enclose the doubly ionizing events with $\mathcal{E}^{mod} = 10$ eV. Panels (b) and (c) are plotted for symmetric E^{mod} energy sharing.

To then determine the two-electron collision time corresponding to a certain excess energy, for instance, $E^{xs} = 10$ (20) eV, the best we can do, according to method 1, is to compute the two-electron collision time of the double-ionization events corresponding to $\mathcal{E}^{mod} = 10$ (20) eV. We do so and determine the collision time for $\mathcal{E}^{mod} = 10$ (20) eV in Figs. 4(a) and 4(c) by extracting $\Delta\phi$ from the lower branch of the interelectronic angle of escape $\theta_{12}(\phi)$; this procedure is described in detail in Refs. [10,12]. We find that $\Delta\phi$ is 4.1° (1.9°), corresponding to a collision time of 2.5 (1.2) a.u. for $\mathcal{E}^{mod} = 10$ (20) eV, respectively. We note that the variation in collision time with excess energy suggests that the accuracy of $\Delta\phi$ depends critically on the resolution in θ_{12}. In order to increase the robustness of the retrieval algorithm we determine $\Delta\phi$ for a range of bin sizes $d\theta_{12} = 4$–9°. We define the average of $\Delta\phi(d\theta_{12})$ as the collision phase or collision time at a given excess energy or $\mathcal{E}^{mod}$.

In Figs. 4(a) and 4(b) we have shown how to obtain the two-electron collision time for $\mathcal{E}^{mod}$ equal to 10 and 20 eV respectively. By repeating the process for excess

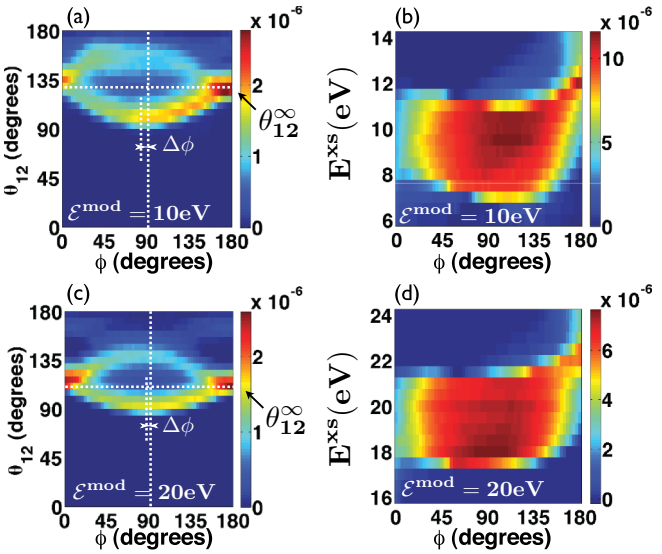

FIG. 4. (Color online) θ_{12} as a function of ϕ for "modified" energies around 10 eV (a) and 20 eV (c) in the presence of the XUV and IR field. $\Delta\phi$ is the shift of the maximum of the vector potential of the IR field, corresponding to a maximum of the split of θ_{12} as a function of ϕ. (b) Excess energies as a function of ϕ that contribute to the "modified" energy around 10 eV enclosed by the white dashed lines in Fig. 3(c) and similarly (not shown) for the "modified" energy centered around 20 eV. Figure 4 is plotted for symmetric E^{mod} energy sharing.

energies ranging from 10 to 56 eV we obtain the collision time for the same range of $\mathcal{E}^{mod}$ energies in Fig. 5(a). We find that the collision time decreases with increasing excess energy, that is, increasing $\mathcal{E}^{mod}$. Since in our computation (but not experimentally) we can identify the double-ionization events in the presence of the XUV and IR fields, which are triggered by only a single excess energy, E^{xs}, we also compute the collision time corresponding to this excess energy; see Fig. 5(a). Figure 5(a) shows that the retrieval algorithm for the collision time based on $\mathcal{E}^{mod}$ works better at lower excess energies. The reason is that we compute the delay times corresponding to a certain $\mathcal{E}^{mod}$ using $\Delta E \approx 8$ eV independent of the excess energy. This choice of ΔE describes best the rate of increase of the "modified" electron energy with ϕ for smaller excess energies. However, ΔE decreases with

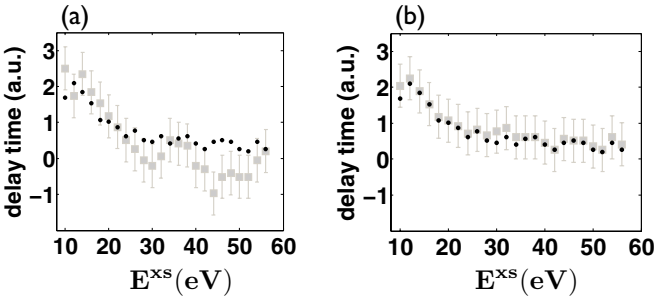

FIG. 5. □ indicates the collision times for "modified" electron energies $\mathcal{E}^{mod}$ from 10 to 56 eV; • indicates the collision times for pure excess energies E^{xs} ranging from 10 to 56 eV. Collision time was retrieved by (a) method 1 and (b) method 2. The error bars show the uncertainty in the delay times of 0.6 a.u. since we change ϕ every 1°.

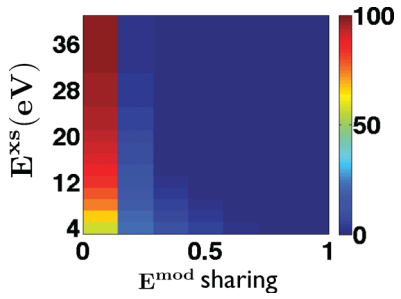

FIG. 6. (Color online) Correlation map of the excess energy with the "modified" energy sharing for the doubly ionizing events with equal energy sharing in the absence of the IR field. The color scale is such that the sum of E^{mod} energy sharings contributing to the equal energy sharing double-ionization events for a certain E^{xs} is normalized to 100.

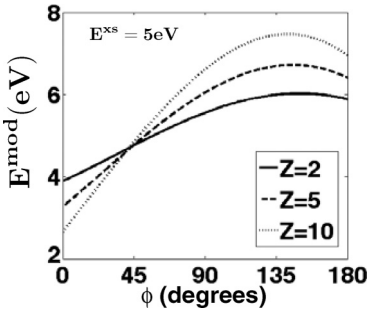

FIG. 7. Average of E^{mod} as a function of ϕ for the one-electron case for $E^{\mathrm{xs}} = 5$ eV for charges $Z = 2,5,10$.

increasing excess energy. As a result, the agreement is worse for higher excess energies.

Accounting for the fact that ΔE changes with excess energy (method 2); we obtain a much better agreement between the two sets of collision time; see Fig. 5(b). One way to do so is by labeling as $\mathcal{E}^{\mathrm{mod}}$ the doubly ionizing trajectories with E^{mod} within ± 1 eV of twice the average E^{mod} for the one-electron problem; see Figs. 3(a) and 3(b). Therefore, in this algorithm we use the calculated E^{mod} as input for each excess energy whereas the previously described algorithm uses only experimentally accessible data. In both algorithms the collision times are computed for symmetric "modified" energy sharing. The reason we choose the symmetric energy sharing in terms of the "modified" energy is that the symmetric "modified" energy sharing is strongly correlated to the symmetric energy sharing in the absence of the IR field (Fig. 6); it is the collision time corresponding to this latter energy sharing that we aim to streak.

Finally, we note that the algorithms described above for obtaining the two-electron collision time, including Eq. (4) and Eq. (5), are applicable to atoms with higher nuclear charge as well. The only difference is that the change of the "modified" electron energy with ϕ gets larger with increasing charge. This is illustrated in Fig. 7 for the one-electron case. For higher charges, in method 2 one would follow the exact same steps as for the case of charge equal to 2 described above. However, for method 1 one would need to consider a larger interval ΔE to correctly account for E^{mod} being steeper as a function of ϕ for larger nuclear charges.

IV. CONCLUSION

In conclusion, we have demonstrated that the two-electron streak camera can be experimentally realized. We obtain a complete picture of the single-photon double-ionization process by computing the two-electron collision times for different excess energies. While our study has been performed in the context of two-electron escape in atoms, it opens the way for time-resolving collision dynamics during multielectron escape in atomic and molecular systems.

ACKNOWLEDGMENTS

A.E. acknowledges support from EPSRC under Grant No. EPSRC/H0031771, from NSF under Grant No. NSF/0855403 and use of the Legion computational resources at UCL.

[1] M. Drescher, M. Hentschel, R. Kienberger, G. Tempea, Ch. Spielmann, G. A. Reider, P. B. Corkum, and F. Krausz, Science **291**, 1923 (2001).

[2] J. Itatani, F. Quéré, G. L. Yudin, M. Yu. Ivanov, F. Krausz, and P. B. Corkum, Phys. Rev. Lett. **88**, 173903 (2002).

[3] Y. Mairesse and F. Quere, Phys. Rev. A **71**, 011401(R) (2005).

[4] K. Klunder, J. M. Dahlstrom, M. Gisselbrecht, T. Fordell, M. Swoboda, D. Guenot, P. Johnsson, J. Caillat, J. Mauritsson, A. Maquet, R. Taieb, and A. L'Huillier, Phys. Rev. Lett. **106**, 143002 (2011).

[5] L. R. Moore, M. A. Lysaght, J. S. Parker, H. W. van der Hart, and K. T. Taylor, Phys. Rev. A **84**, 061404(R) (2011); A. S. Kheifets, I. A. Ivanov, Phys. Rev. Lett. **105**, 233002 (2010).

[6] M. Uiberacker, Th. Uphues, M. Schultze, A. J. Verhoef, V. Yakovlev, M. F. Kling, J. Rauschenberger, N. M. Kabachnik, H. Schröder, M. Lezius, K. L. Kompa, H.-G. Muller, M. J. J. Vrakking, S. Hendel, U. Kleineberg, U. Heinzmann, M. Drescher, and F. Krausz, Nature (London) **446**, 627 (2007).

[7] P. Eckle, A. N. Pfeiffer, C. Cirelli, A. Staudte, R. Dörner, H. G. Muller, M. Büttiker, and U. Keller, Science **322**, 1525 (2008).

[8] M. Schultze *et al.*, Science **328**, 1658 (2010).

[9] A. L. Cavalieri, N. Müller, Th. Uphues, V. S. Yakovlev, A. Baltuska, B. Horvath, B. Schmidt, L. Blümel, R. Holzwarth, S. Hendel, M. Drescher, U. Kleineberg, P. M. Echenique, R. Kienberger, F. Krausz, and U. Heinzmann, Nature (London) **449**, 1029 (2007).

[10] A. Emmanouilidou, A. Staudte, and P. B. Corkum, New J. Phys. **12**, 103024 (2010).

[11] A. Knapp, A. Kheifets, I. Bray, Th. Weber, A. L. Landers, S. Schössler, T. Jahnke, J. Nickles, S. Kammer, O. Jagutzki, L. Ph. H. Schmidt, T. Osipov, J. Rösch, M. H. Prior, H. Schmidt-Böcking, C. L. Cocke, and R. Dörner, Phys. Rev. Lett. **89**, 033004 (2002).

[12] H. Price, A. Staudte, and A. Emmanouilidou, New J. Phys. **13**, 093006 (2011).

[13] *Frequency-Resolved Optical Gating*, edited by R. Trebino (Kluwer Academic, Boston, 2000).

[14] R. Abrines and I. C. Percival, Proc. Phys. Soc. **88**, 861 (1966).
[15] A. Emmanouilidou and J. M. Rost, Phys. Rev. A **75**, 022712 (2007).
[16] A. Emmanouilidou, P. Wang, and J. M. Rost, Phys. Rev. Lett. **100**, 063002 (2008).
[17] A. Emmanouilidou and J. M. Rost, J. Phys. B **39**, 4037 (2006).
[18] D. J. W. Hardie and R. E. Olson, J. Phys. B **16**, 1983 (1983); D. Eichenauer, N. Grün, and W. Scheid, *ibid.* **14**, 3929 (1981); J. S. Cohen, *ibid.* **18**, 1759 (1985).
[19] T. Havermeier, T. Jahnke, K. Kreidi, R. Wallauer, S. Voss, M. Schöffler, S. Schössler, L. Foucar, N. Neumann, J. Titze, H. Sann, M. Kuhnel, J. Voigtsberger, A. Malakzadeh, N. Sisourat, W. Schöllkopf, H. Schmidt-Bocking, R. E. Grisenti, and R. Dörner, Phys. Rev. Lett. **104**, 153401 (2010).
[20] B. H. Bransden and C. J. Joachain, *Physics of Atoms and Molecules* (Pearson, Harlow, Essex, 2003).
[21] H. A. Bethe and E. E. Salpeter, *Quantum Mechanics of One- and Two-Electron Atoms* (Dover, Mineola, New York, 1957).